ARCHIVES
of
FOUNDRY ENGINEERING

ISSN (2299-2944)
Volume 2025
Issue 4/2025

211 – 219

10.24425/afe.2025.157619

26/4

Published quarterly as the organ of the Foundry Commission of the Polish Academy of Sciences

Microstructure Modelling During Heating and Deformation of S355 Steel Samples in the Temperature Range of Phase Transformation Using a Coupled FE/CA/MC Model

T. Dębiński *, M. Hojny
AGH University of Krakow, Poland
* Corresponding author: e-mail: debinski@agh.edu.pl

Received 11.08.25; accepted in revised form 05.12.25; available online 31.12.2025

Abstract

This paper presents, a calculation method to model the material morphology during heating and deformation of samples to temperatures close to the solidus line. Two approaches were used, for heating and heating with deformation. In the first case, only the temperature information of the FEM mesh nodes is transferred to MC model. In the case of heating and deformation, a FE/CA model was proposed where the computational domain is mapped based on the displacement vectors from the FEM mesh. The developed model is a hybrid of the finite element method (FEM) with Monte Carlo (MC) and Random Cellular Automata (RCA) methods. It is used to simulate thermomechanical processes such as resistance heating, local remelting and sample deformation. At the macroscopic level, a modified rigid-plastic model with, a controlled compressibility condition was used. A Gleeble 3800 thermomechanical simulator was used in the study for heating, melting, cooling and deformation experiments off steel samples. Validation of the micro model was perform on metallographic scans and quantitative and qualitative grains analysis. Comparison of the experimental and numerical data made it possible to evaluate the accuracy of the model.

Keywords: Image analysis, Heating simulation, Grain growth, Macrostructure, Morphometric parameters, Numerical simulation

1. Introduction

The intensive development of computer technologies, accompanied by the continuous growth in the computing capacity, enables more and more complex physical processes to be effectively modelled. It allows new computing methods to be applied, which could not be used earlier due to extremely long computing times. A fast development can be observed in the area of the so-called meshfree methods, allowing many physical phenomena to be modelled. Classical material models currently used most often in numerical simulations, are mainly used to analyse material behaviour on a macroscopic scale. In this case, the local interactions of the micro scale on the macro scale are ignored. Failure to take into account the morphology of the microstructure in the numerical model, ultimately translates into the quality of the computer simulation results obtained which will be characterized

by lower precision. Classical materials models most often use models so called mean field models to describe the state of a material for example conventional models of microstructure development based on the JMAK (Johnson-Mehl-Avrami-Kolmogorov) equation, or stress-strain curves describing the stress-strain relationship, possibly by considering additional internal variables, e.g. strain rate, temperature, liquid phase fraction [1-4]. The use of a mean field model description, for example, in modelling metallic materials requires the assumption that the material is polycrystalline and the properties of individual crystallites are homogenized and depend mainly on internal variables. The main disadvantage of macroscopic models is that they treat the material as a single cluster of many millions of grains where their interactions and also individual behaviour are ignored. As a result, the information obtained makes it possible to satisfactorily determine only the global properties of the test product by analysing the distribution of stresses, temperatures or strains. The above approach is sufficient for most metal processing in civil and military applications. Therefore, it can be concluded that the standard modelling approach described above does not meet the requirements of modern materials engineering, which designs and manufactures innovative materials using the relationship between the morphology of the microstructure and the final properties of the end product. Therefore, it is very important to develop a new generation of numerical models that take into account the influence of the components of the microstructure overtly on its evolution, i.e., so called full field models. The defence industry, due to its enormous diversity, finds applications for almost every group of metals and alloys. Among the most important materials are Ni, Ti, Fe, Co, Al, Mo, W, Mg alloys. The introduction of new multiphase steels or the modern alloys mentioned above has necessitated changes in traditional modelling. In modern material modelling, specific properties are obtained through properly designed morphology of their microstructures obtained by controlled thermo-mechanical processing [5]. Thus, modern material modelling during processing (e.g. large deformation, heat treatment) is based on the observation that the measured response of a material depends on microstructural features such as grain size, porosity, phase boundaries, grain boundaries, inclusions). One practical approach to advanced modelling with considerations of microstructural aspects is to apply the concept of Digital Material Representation (DMR) which can be combined with models based on discrete methods such as Random Cellular Automata (RCA) or Monte Carlo (MC). To date, scientific research in the use of the Random Cellular Automata method has been concerned with simulating the development of microstructure mainly after deformation [6-13], where the problem of modelling the deformation of the computational domain has not been considered due to the complexity in terms of reliable representation of the computational domain during deformation [14,15]. In the literature one can find more than a dozen scientific papers where the main goal was to develop methods for reliable representation of the deformation domain [16-20]. These solutions are most often based on simplifications and the combination of the Random Cellular Automata method with the finite element method (FEM). The simplifications used in the algorithms for mapping the computational space and the complexity of the model at the micro-macro level led to unacceptable quality of results, as well as extremely long calculation times. These problems fundamentally limited the use of the developed multiscale models in practice (as well as subsequent transfer to industry). The proposed hybrid solution concept assumes such a combination of the three methods, where the position of the cellular automata cells is modified using the node displacement vectors of the finite element method, such an assumption will guarantee, a reliable computational domain deformation mechanism. The developed solution will allow precise determination of geometric and morphological changes at the microstructural level during modelling of materials subjected to deformation.

2. Mathematical model

2.1. Thermo-mechanical model

The developed multi-scale model is a hybrid solution combining the finite element (FE) method with Monte Carlo (MC) and Random Cellular Automata (RCA) method. The finite element method is the basis of the thermo-mechanical solution for the macroscale in aspects of simulating resistive heating combined with local remelting and deformation of the sample. The strain field and stress deviator for the spatially and axisymmetric deformation state were determined using a modified rigid-plastic model of a continuous medium. A modification of the classical rigid-plastic solution [21,23] consisted in replacing the incompressibility (volume conservation) condition with a controlled compressibility condition, which is described by the operator equation (1):

$$\nabla \bar{v} = \frac{1}{\rho}\frac{\partial \rho}{\partial \tau} \tag{1}$$

where: $\bar{v} = \left(v_x, v_y, v_z\right)$ - velocity vector field, ρ -density, τ - time.

and the rigid-plastic solution functional takes the following form (2):

$$J\left[\bar{v}\right] = \int_{\Omega} \sigma_p \dot{\varepsilon}_i d\Omega + \int_{\Omega} \lambda \left(\nabla \bar{v} - \frac{1}{\rho}\frac{\partial \rho}{\partial \tau} \right) d\Omega \tag{2}$$

where: σ_p - yield stress, $\dot{\varepsilon}_i$ - strain rate intensity, Ω - the volume of the considered medium, λ - penalty factor.

The temperature field for unsteady heat conduction without convection was determined by solving the Fourier–Kirchhoff equation, which, without heat advection, can be written as: (3) [21,23]:

$$k\left(\frac{\partial^2 T}{\partial x^2} + \frac{\partial^2 T}{\partial y^2} + \frac{\partial^2 T}{\partial z^2} \right) + \left(Q - \rho c_p \frac{\partial T}{\partial \tau} \right) = 0 \tag{3}$$

where: k -thermal conductivity, T -temperature, Q -heat generation rate, c_p -specific heat.

The solution of Eq. (3) requires the correct specification of boundary and initial conditions. The boundary conditions were adapted according to the experimental setup in the Gleeble 3800 thermo-mechanical simulator system. The details of the solution are presented in the publication [21].

2.2. Grain Growth Model

The mathematical model at the microscale level is based on the application of Monte Carlo (MC) and Random Cellular Automata (RCA) methods for simulating grain growth.
In the initial stage of the process comprising heating/remelting followed by cooling to the deformation temperature an algorithm based on the MC method is applied (at the current stage of development, the model has a probabilistic character).
The implemented MC algorithm is based on the minimization of the system's energy, in which local energy changes are calculated using the Hamiltonian (4) to calculate the system's energy, which is then employed to determine the probability of a change in the state of a cell. A single cell is randomly selected from the automaton domain and checked for a possible change in affiliation to another grain, corresponding to either grain growth or absorption by a neighbouring grain. The direction of growth depends on both the boundary energy change and temperature; therefore, neighbouring cells with the same orientation as the 'base' cell are identified.

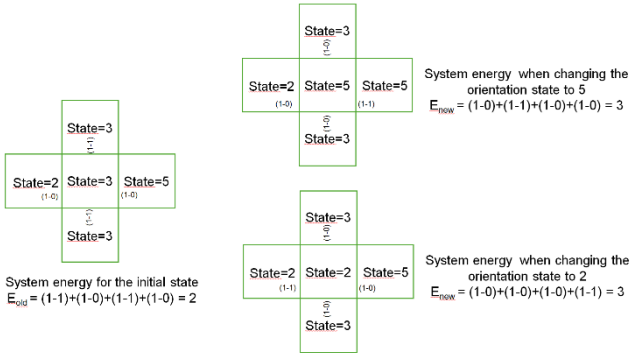

Fig. 1. System energy for different orientation states

The energy change is calculated for each possible state transition (fig. 1). One may select the change corresponding to the smallest ΔE, however, by using a probability function, it is also possible to determine the likelihood of a state change.

$$E = J \sum_{\langle i_m, j_m \rangle} \left(1 - \delta_{i_m j_m}\right) \tag{4}$$

where: J -grain boundary energy, δ -Kronecker delta, i_m, j_m -cell and neighbour number.
The overall procedure of the coupled FE/MC approach is implemented as follows:

1) Simulation of heating/remelting/cooling to determine the temperature field distribution within the sample volume (macro model) [17],
2) Interpolation of nodal temperatures from the finite element mesh of the macro model onto the cells of the micro model (for given integration steps) [17,19,20],
3) Random selection of cells and an attempt to change their state (identifier Q_{grain} defining membership to a specific grain orientation),
4) The state change is accepted with a probability of P :

$$P = B_m(T) e^{-\frac{\Delta E}{kT}} \qquad \Delta E > 0 \tag{5}$$

$$P = B_m(T) \qquad \Delta E \le 0 \tag{6}$$

where: P -probability function, B_m -boundary mobility function, ΔE -change of energy, kT -modelling parameter.

In equations (5) and (6) $B_m(T)$ is the boundary mobility function that accounts for the varying temperature values in different regions of the sample volume affecting the probability value. In the calculations, the boundary mobility function was assumed to have the following form (7):

$$B_m(T) = \frac{(T-20)^3}{(T_l-20)^3} \tag{7}$$

where: T_s, T_l -solidus and liquidus temperature.

The details of the solution are presented in the publication [21].In the second stage of the modelling procedure, the created microstructure is used in the algorithm for generating the cellular automata space. It is the initial condition in the RCAFE (Random Cellular Automata – Finite Element) model of steel deformation in the semi-solid state. The neighbourhood in the RCA algorithm is based on a fixed radius R, using transition rules developed by Liang [22]. It is assumed that the transformation of the RCA domain in the micro model follows the same transformation laws as the finite elements in the macro model. During the deformation simulation (the third stage), temperature and displacement vectors are mapped (interpolated) onto individual RCA cells, based on which the transformation of the RCA domain is performed.
In each iteration of a cellular automata, the state of each cell depends on the states of its neighbours and its own state. The state change depends on precisely defined transition rules (8):

$$Y_{i,j}^{t+1} = \text{if } \Lambda \text{ is a new state, then } Y_{i,j}^{t} \tag{8}$$

where: $Y_{i,j}^{t+1}, Y_{i,j}^{t}$ – *cell states i, j in the current and previous time steps,* Λ - *logical function* (9):

$$\Lambda = \Lambda(Y_{i,j}^{t}, Y_{k,l}^{t}, p, q) \tag{9}$$

where: $Y_{k,l}^{t}$ – *the state of cells k, l neighbouring cells i and j in the previous time step,* ***p, q*** – *vectors containing external and internal variables.*

The behavior of the entire CA is determined by strictly defined transition rules. The numerical algorithm controls the position of each automaton within the volume of the respective finite elements. In case of overlap or if a cell moves outside the volume to which it belongs, the algorithm reports an error and terminates the calculations. The estimated value of the liquid phase fraction f_l from the micro model is used to calculate the value of the yield stress σ (10) for individual elements of the deformation zone at the macro model level.

$$\sigma = \frac{\varepsilon^n}{\alpha} ASINH\left[\left(\frac{\dot{\varepsilon}}{A}\right)^m \exp\left(\frac{mQ}{RT}\right)\right]\left[(1-\beta f_l)^k\right] \qquad (10)$$

where: $\alpha, \beta, A, m, n, k$ are parameters of the yield stress function T is the temperature, R is a gas constant (8.314 J/molK), f_l is the liquid phase fraction.

In third stage, due to the long computation time and the inclusion of deformation, a modified RCA method was used. The process diagram is shown in the figure 2.

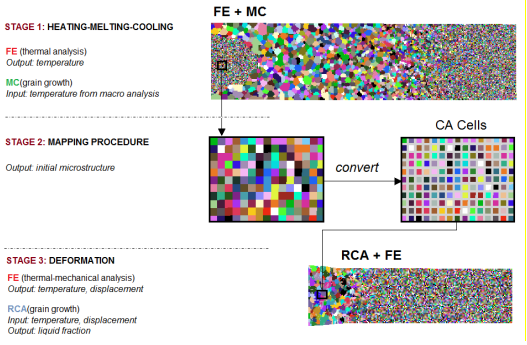

Fig. 2. Stages of data transfer from the FE+MC method (heating, melting, cooling) to RCA+FE (deformation)

3. Experimental methodology

The heating, melting, and controlled cooling experiments were performed using the Gleeble thermomechanical simulator [24]. The objective was to conduct tests using small samples made from the material used in the actual production process. The results of the thermomechanical parameter analysis for various types of simulations can also be useful for optimizing the operating parameters of the technological line equipment.

The chemical composition of the tested S3555 steel is presented in Table 1. The characteristic solidus and liquidus temperatures were 1465°C and 1513°C, respectively.

Table 1.
Chemical composition of the tested steel (in %)

C	Ni	P	Si	Mn	Cr	S
0.16	0.06	0.011	0.26	1.26	0.14	0.009

Samples with a square cross-section measuring 10×10×124 mm were used. Figure 3 shows, a schematic of the sample with the location of temperature measurement points (thermocouples) and the division into zones of heat exchange with the environment.

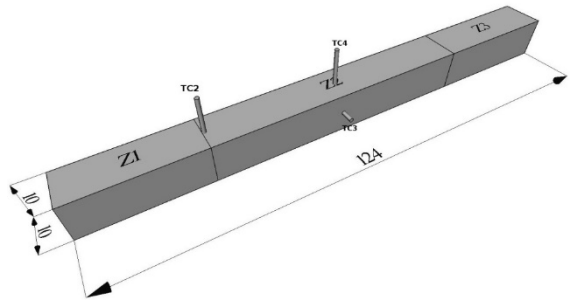

Fig. 3. Sample diagram along with the location of thermocouples (TC2, TC3, TC4) and heat transfer zones (Z1, Z2, Z3)

The Z2 zone shown in the figure indicates the area of the sample where free heat exchange with the environment occurs and zones Z1 and Z3 represent the areas in contact with the water-cooled copper grips. The characteristic temperatures were measured at specific locations shown in Figure 3. Thermocouple TC3 provided information about the temperature in the core of the sample, while two additional thermocouples were used to record temperature changes on the sample surface in the central part (TC4) and near the grips (TC2).

Based on the material data and the known characteristic solidus and liquidus temperatures, the process of direct heating, holding, and cooling of the sample was performed according to a precisely specified scenario. The sample was heated at a constant rate of 5 °C/s up to a temperature of 1440 °C. Cooling was carried out down to a nominal temperature of 800°C at a rate of 10°C/s, and then continued to room temperature. During the experiment, temperatures were recorded continuously using all thermocouples. For equipment reasons, in the core of the sample, temperature measurements were possible up to 1200°C. Above this, up to 1440°C, the temperature was estimated based on previously obtained experimental data.

4. Experimental verification

4.1. Modelling of microstructural morphology during heating

In the Gleeble 3800 thermomechanical simulator, resistive heating causes a heterogeneous temperature field to develop inside the sample [21]. In the temperature range close to the solidus line, slight local temperature variations can rapidly change the mechanical properties. This has a direct impact on the accuracy of force parameter predictions and on the size and geometry of the resulting deformation zone. Figure 4 shows the calculated temperature fields at selected stages during heating to the nominal temperature of 1440°C.

Analysis of the results shows that the temperature difference between the sample surface and its core (located at half the length of the heating zone) increases with rising heating temperature.

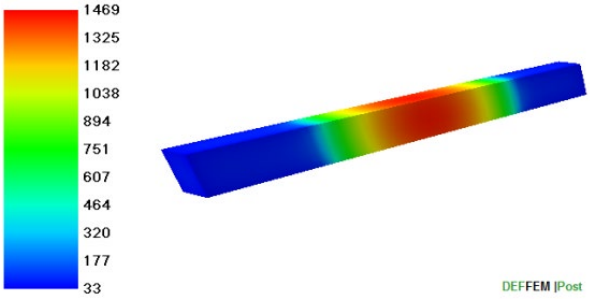

Fig. 4. Temperature field obtained from resistance heating to nominal temperature 1440°C

The maximum core temperature of the sample, reaching 1469°C, was attained during the heating stage to a nominal temperature of 1435°C, which led to local melting of the sample and the formation of a zone consisting of a mixture of liquid and solid phases.

Table 2.
Comparison of measured and calculated temperature differences between the core and the surface of the sample

Experiment, (°C)						
TC4	100	300	500	800	1200	1435
TC3	105.68	305.40	507.37	816.32	1226.22	1481.47
TC3-TC4	**5.68**	**5.40**	**7.37**	**16.32**	**26.22**	**46.47**
Simulation, (°C)						
NTC4	100	300	500	800	1200	1435
NTC3	102.99	304.64	511.98	818.19	1229.11	1469.18
NTC3-NTC4	**2.99**	**4.64**	**11.98**	**18.19**	**29.11**	**34.18**

Table 2 summarizes the calculated and measured temperature differences between the core and the surface of the sample. More details regarding the verification of the resistive heating model are presented in reference [21].

Figure 5 shows example digital representations of the microstructure (result of numerical simulation) obtained on the cross-section of the sample at half the length of the heating zone, with the visible formed mixed zone in the core of the sample during its melting stage. The final stage of the simulation was free cooling of the sample in the tooling system of the Gleeble 3800 simulator (no deformation was applied). This results in a fine-grained morphology due to the high cooling rates.

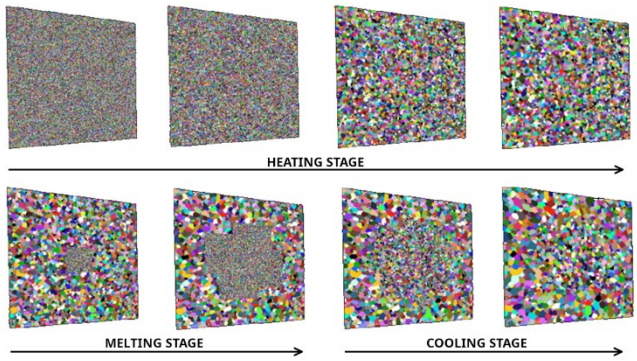

Fig. 5. Digital representation of the macrostructure on the cross-section of the sample (at half the length of the heating zone) for selected stages of integrated heating combined with local melting and free cooling

During the experimental studies, metallographic specimens were prepared on selected longitudinal sections (the central part of the sample and at distances of 5 and 10 mm from the sample core) and cross-section sections (the core and at a distance of 10 mm from the sample core). These selected locations for specimen preparation allowed for preliminary verification and qualitative assessment of the results obtained from the micro model. Figure 6 presents the procedural steps for a cross-section (central part of the sample, experiment). Based on a qualitative evaluation of the obtained microstructure from the experiment (Fig.6A), it can be concluded that grains detection may be difficult.

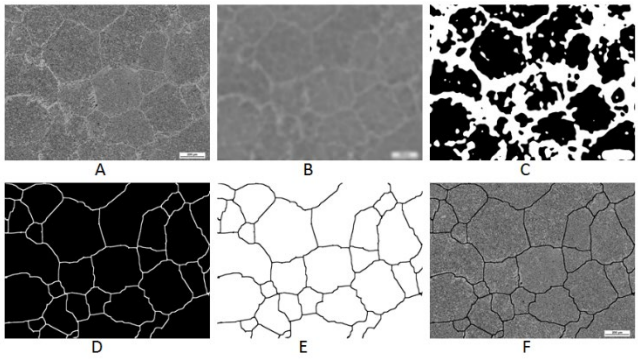

Fig. 6. Stages of microstructure processing using ImageJ software, A) contrast adjustment, B) blurring, C) binarization with thresholding, D) skeletonization, reconstruction, dilation, E) inversion, F) final image

Performing binarization does not allow the detection of grain boundaries, however, it does allow observed inhomogeneities in image brightness, so in order to extract details from the image at a uniform level, a local contrast enhancement operation was performed (Fig.6A). In order to remove noise occurring inside the grains, it was decided to use a Gaussian filter, which is characterised by a monotonically decreasing impulse response (as a function of frequency) and thus introduces much less distortion in the image, especially at the edges of objects (Fig.6B). The next step was a binarization operation by thresholding with an appropriately selected range (Fig.6C). The next step was a

skeletisation to find the boundaries of the objects. As the resulting mesh shows many discontinuities, a dilation with a step of 1 was used and objects that are not in contact with the image mesh were removed. Finally, conditional reconstruction was used (Fig.6D). The final step is color inversion (Fig. 6E) and overlaying the detected grain boundaries onto the original microstructure image (Fig. 6F). The digital representations of the microstructure (calculated) were analysed according to the proposed methodology used for the microstructures from the experiment (Fig. 7). The figure shows the result of digital reconstruction of the microstructure after cooling. This result was obtained after calibration of the proposed methodology. It shows different grain growth dynamics depending on the sample area.

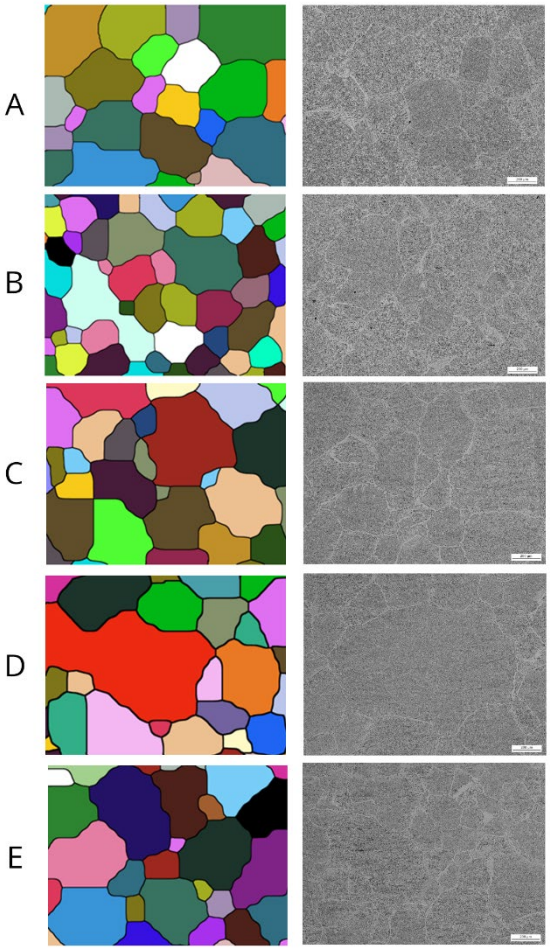

Fig. 7. Digital representation of the microstructure and metallographic experimental images on selected: A) cross section 0mm, B) cross section 10mm, C) longitudinal section 0mm, D) longitudinal section 5mm, E) longitudinal section 10mm

The primary parameters used for the preliminary verification of the developed grain micro-growth model are the number and size (surface area) of grains in the visible area. There are many algorithms and methods for determining these values. In the presented research results, a recursive image segmentation method (identification of connected regions) was chosen. Additionally, selected morphometric parameters were determined, such as the average grain surface area, average height and width, average circularity, aspect ratio, roundness, and compactness with the following equations:

$$circularity = 4\pi \frac{A}{p^2} \tag{11}$$

$$AR(aspectratio) = \frac{major\ axis}{mior\ axis} \tag{12}$$

$$Round(roundness) \frac{4A}{\pi(major\ axis)^2} \tag{13}$$

$$Solidity = \frac{A}{A_{convex\ hull}} \tag{14}$$

where: A - grain surface area, p - grain circuit, $major, mior$ - axes of the fitted ellipse, $A_{convex\ hull}$ - convex hull surface area.

For microstructure image processing and morphometric parameter calculations, the ImageJ software was used.

Morphometric analysis parameters were determined for both the structures obtained experimentally and those generated through numerical modelling (Fig. 8). For each microstructure, the number of visible grains was determined and then compared with the results from the numerical simulation.

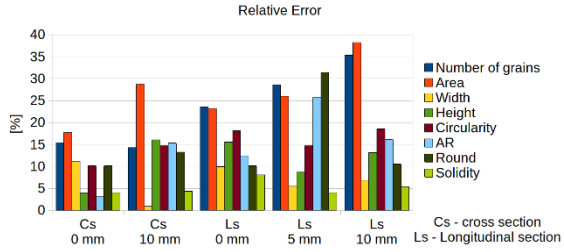

Fig. 8. Relative error determining of morphological parameters between experiment and calculations

Grains located at the edges of the image were excluded from the analysis. The main problem was the inhomogeneity caused by the high fragmentation of the structure within the grains, which made the detection of their boundaries difficult and caused, in some cases, significant differences in the values of individual morphometric parameters. The maximum value of the relative error in such cases exceeded the value of 25% (4 cases), while in other cases it was in the range of 5 - 20%.

4.2. Modelling morphology during deformation

Deformation simulations (micro model only) for temperatures higher than 1445°C with a 5 mm compression were unsuccessful. The mixed zone occurring in the core of the sample, which was the area of greatest deformation, was also the area where a large

deformation of the finite element mesh occurred. As a result, this led to a lack of convergence of the optimisation procedures and the calculation was interrupted. It was also not possible to perform deformation calculations for temperatures below 1435°C with the micro model. With such a large compression (5 mm), it was difficult to control the position of a given cellular automata in the volume of the individual finite elements. This led to frequent overlapping of cellular automata one on top of the other, or going outside the finite element area. As a result, the range of applicability of the developed numerical models was determined. For deformation simulations that do not include a micro model, the limits are a stroke of 5 mm and a maximum (nominal) deformation temperature of 1445°C. This results in a maximum achievable value for the fraction of the liquid phase in the sample volume $f_l = 0.2$ (maximum temperature of the sample core 1475°C). For the deformation simulation variant including the micro model, the pre-estimated limit is a stroke of 1.2 mm and a maximum (nominal) deformation temperature of 1435°C. This results in a maximum achievable value for the fraction of the liquid phase in the sample volume $f_l = 0.1$ (maximum temperature of the sample core 1470°C). Figs. 9 and 10 show the strain values in the X-axis direction for 1435°C and 1450°C respectively.

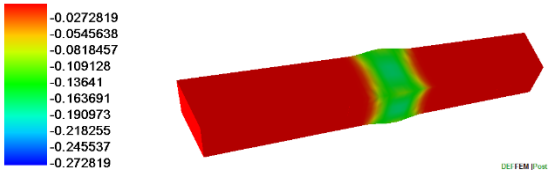

Fig. 9. Strain value in the X axis direction for a temperature of 1435°C

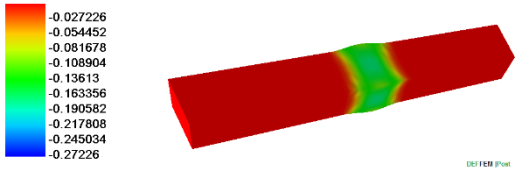

Fig. 10. Strain value in the X axis direction for a temperature of 1450°C

Fig. 11 and Fig. 12 show, respectively, the temperature field after heating the sample to a nominal strain temperature of 1435°C and the resulting digital representation of the macrostructure on the longitudinal section.

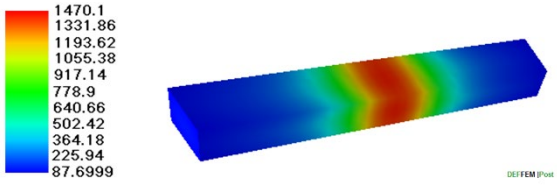

Fig. 11. Temperature field obtained by resistance heating to a nominal temperature of 1435 °C (76 mm sample length)

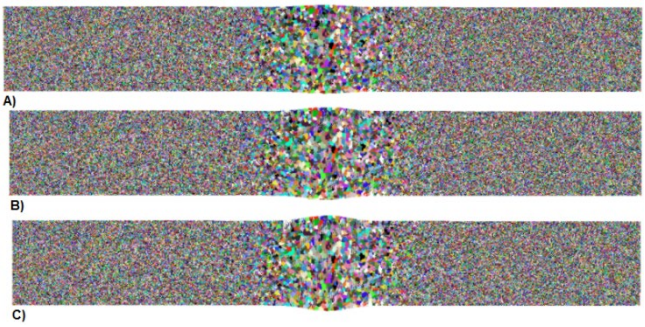

Fig. 12. Digital representation of the macrostructure on the longitudinal section of a sample deformed at 1435 °C (sample length 76 mm, stroke 1.2 mm)

By analysing the digital representation of the macrostructure obtained on the longitudinal section (Fig.12), it can be observed that the area with the highest grain growth dynamics is the free area of the sample. This is where the highest intensity of heat release due to resistance heating occurs. In the case of the 76 mm long sample used, the length of the free zone L_{fz} is ~15.5 mm. In the contact area between the sample and the copper tools, the structural state matches the structure of the input state.

In order to obtain a quantitative assessment of the mixed structure, it is necessary to determine the size of the temperature-affected zones in the sample image from experiment. Due to the complexity of the operation, an assessment was performed to select the levels of binarisation, the filter to extract the zones of complete remelting, the mixed zone and the heat-affected zone (solid).

The first step before the analysis is to reduce image details and filter out noise. The macroscopic images used are characterized by the presence of small grains and varying brightness levels of structural elements. The task is to select the appropriate filtering and segmentation steps to identify the zone areas. Subsequent image processing extracts the identified regions and produces an image of the zones with a continuous, uniform distribution of grey levels and brightness that differs from that of neighbouring zones. To remove redundant information from the image, pre- and intermediate filtering were performed in the following steps: a median filter (mask size 10), a morphological closing filter (circular mask with a radius of 10), and finally, contrast stretching. Figure 13 shows the longitudinal scan after the applied filtering steps. The yellow line indicates the vector along which the brightness profile of the sample was analysed.

For the filtering methodology chosen in this way, an image with highlighted phase areas and a significant reduction in noise was obtained.

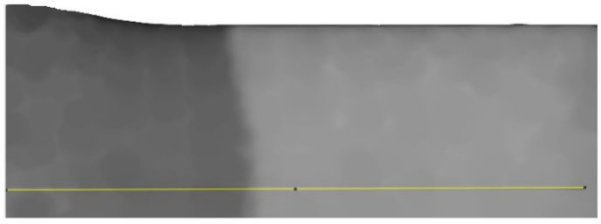

Fig. 13. Image after processing, before binarisation

Table 3 presents the results of determining brightness values for the binarisation process, along with the classification of the identified areas into their respective zones.

Table 3.
Image brightness ranges after binarisation with zones

Area No.	Pixels brightness range		Zone	Start of zone in relation to sample symmetry axis[mm]
	Min	Max		
1	0.49	0.5	Yellow	0
2	0.42	0.49	Violet	0.27
3	0.37	0.42	Blue	1.86
4	0.35	0.37	Green	4.59
5	0.35	0.62	Red	5.73

Fig. 14 shows a summary of the binarisation results obtained and the corresponding zones: 5.red - solid, 4.green - grips cooling-affected zone, 3.blue - ambient cooling-affected zone, 2. purple - transition zone, 1.yellow - complete remelting.

The histogram of the brightness distribution along the vector indicated by the yellow line in Fig. 13 is also presented.

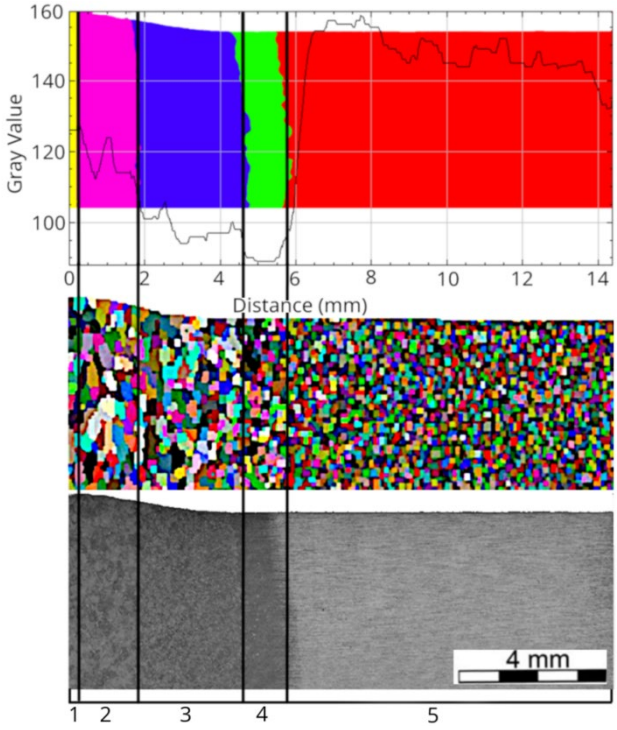

Fig. 14. Image of the different zones according to the ranges shown in Table 3, the histogram of brightness changes along the test vector, and their relation to the sample from both simulation and experiment

This enabled the identification of heat-affected zones based on the experimental results and their projection onto the sample model, together with the microstructure derived from numerical simulation.

4. Conclusions

This paper presents a hybrid computational model combining FEM, Monte Carlo and RCA methods for simulating thermomechanical processes such as heating, remelting and deformation of steel samples. At the macro level, a modified rigid-plastic model was used, and at the micro level, grain growth simulations were used. In the case of deformation, data from the finite element method was transferred to the RCA method in the form of displacement vectors. The research was performed using a Gleeble 3800 simulator. The analysis showed a strong effect of local temperature changes on mechanical properties. Model verification was performed using metallographic samples and grains morphometric analysis. Image processing made it possible to evaluate the accuracy of the model and to reconstruct the microstructure. For the quantitative evaluation of the mixed structure, the temperature-affected zones were determined from the sample image

A comparison of the morphometric parameters and structures obtained from the experiment and the computational model for its verification revealed certain differences, which are presented as the relative error in the determination of individual parameters. The parameters collected from both experimental samples and simulations allowed for the validation of the proposed numerical model of grain growth in high-temperature processes. For improve the accuracy of numerical modelling, research is being conducted using a nonlinear probability function in the Random Cellular Automata (RCA) model. Due to long computation times, studies are also being performed on parallelizing computational model using GPU acceleration.

Acknowledgements

The work was realized as a part of fundamental research financed by the Ministry of Science and Higher Education, grant no. 16.16.110.663.

References

[1] Szeliga, D., Bzowski, K., Rauch, Ł., Kuziak, R. & Pietrzyk, M. (2020). Mean field and full field modelling of microstructure evolution and phase transformations during hot forming and cooling of low carbon steels. *Computer Methods in Materials Science*. 20(3), 121-132. https://doi.org/10.7494/cmms.2020.3.0727.

[2] Avrami, M. (1939). Kinetics of phase change. I: General theory. *The Journal of Chemical Physics.* 7(12), 1103-1112. DOI: 10.1063/1.1750380.

[3] Pietrzyk, M., Szeliga, D. & Kuziak, R. (2014). Physical and numerical simulation of the continuous annealing of DP steel strips. *Steel Research International*. 85(1), 99-111, DOI:10.1002/srin.201200318.

[4] Szeliga, D., Foryś, J., Kusiak, J., Kuziak, R., Nadolski, R., Oprocha, P., Pietrzyk, M., Potorski, P., Rauch, Ł. & Zalecki, W. (2025). Stochastic model of accelerated cooling of eutectoid steel rails. *Modelling and Simulation in Materials Science and*

Engineering, 33(2), 025008, 1-19. DOI: 10.1088/1361-651X/ada81c.

[5] Ludwig, A., Wu, M. & Kharicha, A. (2016). Simulation in metallurgical processing: recent developments and future perspectives. *JOM*. 68(8), 2191-2197. https://doi.org/10.1007/s11837-016-1992-0.

[6] Arun Babu, K., Prithiv, T.S., Gupta, A. & Mandal, S. (2021). Modeling and simulation of dynamic recrystallization in super austenitic stainless steel employing combined cellular automaton, artificial neural network and finite element method. *Computational Materials Science.* 195, 110482, 1-17. DOI: https://doi.org/10.1016/j.commatsci.2021.110482.

[7] Majta, J., Madej, Ł., Svyetlichnyy, D. S., Perzyński, K., Kwiecień, M. & Muszka, K. (2016). Modeling of the inhomogeneity of grain refinement during combined metal forming process by finite element and cellular automata methods. *Materials Science and Engineering*. 671, 204-213. https://doi.org/10.1016/j.msea.2016.06.052.

[8] Ren, X., Huo, Y., Hosseini, S.R.E., He, T., Yan, Z., Fernandes, F. A., Pereira, A.B., Ji, H., Bai, J., Bian, Z. & Du, X. (2023). A multi-scale modelling by coupling cellular automata with finite element method and its application on cross-wedge rolling. *Materials today Communications*. 37, 106976, 1-11. https://doi.org/10.1016/j.mtcomm.2023.106976.

[9] Fang, D.O.N.G., Zhang, T. & Lei, L.I.U. (2023). Multi-scale simulation of flow behavior and microstructure evolution for AA2219 alloy during multi-pass ring rolling process. *Transactions of Nonferrous Metals Society of China*. 33(10), 2926-2942. https://doi.org/10.1016/S1003-6326(23)66308-3.

[10] Mede, T., Kocjan, A., Paulin, I. & Godec, M. (2020). Numerical mesoscale modelling of microstructure evolution during selective laser melting. *Metals*. 10(6), 800, 1-15. https://doi.org/10.3390/met10060800.

[11] Madej, L., Sieradzki, L., Sitko, M., Perzynski, K., Radwanski, K. & Kuziak, R. (2013). Multi scale cellular automata and finite element based model for cold deformation and annealing of a ferritic–pearlitic microstructure. *Computational Materials Science*. 77, 172-181. https://doi.org/10.1016/j.commatsci.2013.04.020.

[12] Duan, X., Wang, M., Che, X., He, L. & Liu, J. (2023). Cellular automata coupled finite element simulation for dynamic recrystallization of extruded AZ80A magnesium alloy. *Journal of Materials Science*. 58, 1345-1367. https://doi.org/10.1007/s10853-022-08069-9.

[13] Chen, F., Zhu, H., Chen, W., Ou, H. & Cui, Z. (2021). Multiscale modeling of discontinuous dynamic recrystallization during hot working by coupling multilevel cellular automaton and finite element method. *International Journal of Plasticity*. 145, 103064, 1-24. https://doi.org/10.1016/j.ijplas.2021.103064.

[14] Zhi, Y., Jiang, Y., Ke, D., Hu, X. & Liu, X. (2024). Review on cellular automata for microstructure simulation of metallic materials. *Materials*. 17(6), 1370, 1-38. https://doi.org/10.3390/ma17061370.

[15] Zhang, Y. & Zhang, J. (2019). Modeling of solidification microstructure evolution in laser powder bed fusion fabricated 316L stainless steel using combined computational fluid dynamics and cellular automata. *Additive Manufacturing*. 28, 750-765. https://doi.org/10.1016/j.addma.2019.06.024.

[16] Wu, C., Jia, B. & Han, S. (2019). Coupling a cellular automaton model with a finite element model for simulating deformation and recrystallization of a low-carbon micro-alloyed steel during hot compression. *Journal of Materials Engineering and Performance.* 28, 938-955. https://doi.org/10.1007/s11665-018-3834-4.

[17] Bakhtiari, M. & Salehi, M.S. (2018). Reconstruction of deformed microstructure using cellular automata method. *Computational Materials Science*. 149, 1-13. https://doi.org/10.1016/j.commatsci.2018.02.053.

[18] Łach, Ł. (2021). Modeling of microstructure evolution during deformation processes by cellular automata—boundary conditions and space reorganization aspects. *Materials*. 14(6), 1377, 1-22. https://doi.org/10.3390/ma14061377.

[19] Sitko, M. & Madej, Ł. (2016). Modelling of the cellular automata space deformation within the RCAFE framework. *AIP Conference Proceedings.* 1769, 160004. https://doi.org/10.1063/1.4963547.

[20] Svyetlichnyy, D.S. (2012). Reorganization of cellular space during the modeling of the microstructure evolution by frontal cellular automata. *Computational Materials Science*. 60, 153-162. https://doi.org/10.1016/j.commatsci.2012.03.029.

[21] Hojny, M. (2018). *Modeling steel deformation in the semi-solid state*. Switzerland: Springer.

[22] Liang Yu, L., Wu, L.S., Li, L.S. & Dong, Y. C. (2008). A cellular automata model for dendrite structure simulation. *Materials Science Forum*. 575-578, 109-114. https://doi.org/10.4028/www.scientific.net/MSF.575-578.109.

[23] Hojny, M. & Dębiński, T. (2022). A novel FE/MC-based mathematical model of mushy steel deformation with GPU support. *Archives of Metallurgy and Materials*. 67(2), 735-742. DOI: https://doi.org/10.24425/amm.2022.137812

[24] Hojny, M., Głowacki, M., Bała, P., Bednarczyk, W. & Zalecki, W. (2019). A multiscale model of heating-remelting-cooling in the Gleeble 3800 thermo-mechanical simulator system. *Archives of Metallurgy and Materials*. 64(1), 401-412. DOI: 10.24425/amm.2019.126266.